Veterinary Microbiology 316 (2026) 110964

Contents lists available at ScienceDirect

Veterinary Microbiology

journal homepage: www.elsevier.com/locate/vetmic

Engineering bright and genetically stable fluorescent *Streptococcus suis* strains for functional in vitro and in vivo applications

Luis Saralegui [a,b], Carla García [a,b], Paula Jurado [a,b], Camila Bosch [a,b], Marga van Setten [c], Vloet Wessel [c], Rocío Bermúdez [d], Clara Marín [b,e], Jesús Arenas [a,b,c,*]

[a] Unit of Microbiology and Immunology, Faculty of Veterinary, University of Zaragoza, Zaragoza, Spain
[b] Agrofood Research University Institute of Aragon (IA2), Zaragoza, Spain
[c] Wageningen BioVeterinary Research, Lelystad, the Netherlands
[d] Department of Pathology Anatomy, Hospital Clínico Universitario Lozano Blesa, Zaragoza, Spain
[e] Department of Animal Science, Agrofood Research and Technology Centre of Aragon (CITA), Zaragoza, Spain

ARTICLE INFO

Keywords:
Streptococcus suis
Fluorescent labeling
SfGFP
Host-pathogen interaction
Genetic engineering

ABSTRACT

Streptococcus suis is a major cause of streptococcal infections in pigs and an emerging zoonotic pathogen, resulting in substantial economic losses in the swine production industry. The limited efficacy of current vaccine strategies and the rise in antimicrobial resistance have intensified efforts to investigate the biology and pathogenesis of the microorganism as a basis for developing alternative control strategies. In this work, we engineered a genetically stable *S. suis* strain producing a superfolder green fluorescent protein that may serve to study this pathogen in a variety of in vitro and in vivo assays. Multiple *S. suis* strains from different genetic backgrounds were successfully transformed, exhibiting strong and stable fluorescence without compromising bacterial growth. Fluorescence intensity remained consistent over 15 serial passages in culture without the need for antibiotic selection, supporting its suitability for long-term experiments. The fluorescent strains were nicely distinguishable by fluorescence microscopy and enabled the detailed study of various biological aspects, including biofilm formation, interactions with eukaryotic cells, and differential growth. In murine infection models, the engineered strains caused streptococcal disease, unlike unencapsulated mutant derivatives, and were detected in internal organs via fluorescence microscopy. Altogether, this work provides a valuable tool for advancing research into *S. suis*.

1. Introduction

S. suis is the causative agent of streptococcal disease in pigs, a systemic infection that is a major cause of morbidity and mortality in intensive pig production farms. The colonization rate can be up to 100%. In Europe, it has been estimated that 60–80% of pig production units are clinically affected with *S. suis* (Neila-Ibáñez et al., 2021). Although this bacterium is a commensal colonizer of the pig nasopharynx, under certain conditions, it can breach mucosal barriers and enter the bloodstream, leading to arthritis, septicemia, endocarditis, or meningitis (Vötsch et al., 2018). In addition to its impact on animal health, *S. suis* is also an emerging zoonotic pathogen. Human infections usually occur through direct contact with infected pigs or the consumption of pig-derived products (Huong et al., 2014; Brizuela et al., 2024; Goyette-Desjardins et al., 2014). *S. suis* is classified into serotypes based on the composition of its capsular polysaccharide. Up to 29 serotypes have been described so far. However, invasive disease is primarily associated with seven capsule types (1, 1/2, 2, 3, 7, 9 and 14), among which serotypes 2 and 9 are the most prevalent worldwide (Goyette-Desjardins et al., 2014).

Antibiotics play a critical role in the treatment of *S. suis* infections. However, their overuse has resulted in the emergence of multi-drug resistant *S. suis* isolates. Our analysis covering the period from 1998 to 2021 reveals high global resistance rates in clinical isolates from pigs, particularly against tetracyclines, lincosamides, and macrolides (Uruén et al., 2022). Current vaccination strategies primarily rely on commercial whole cells or bacterins (Segura, 2015), but these have demonstrated limited efficacy under controlled experimental conditions (Corsaut et al., 2020; Rieckmann et al., 2020). Nonetheless, significant research efforts continue to focus on the development of effective

* Correspondence to: Unit of Microbiology, Immunology, Faculty of Veterinary, University of Zaragoza, Miguel Servet, 177, Zaragoza 50017, Spain.
E-mail address: jaarenas@unizar.es (J. Arenas).

https://doi.org/10.1016/j.vetmic.2026.110964
Received 2 July 2025; Received in revised form 24 February 2026; Accepted 1 March 2026
Available online 2 March 2026

vaccines and novel antimicrobial agents.

Understanding host colonization, pathogenesis and susceptibility or resistance to novel antimicrobial agents is essential for developing new strategies and identifying effective substances to combat *S. suis* infections. Notably, *S. suis* exhibits considerable genetic and phenotypic diversity (Weinert et al., 2015; Guo et al., 2021; Uruén et al., 2024) and its pathogenesis involves a wide range of structures that facilitate the dissemination and disease progression (Fittipaldi et al., 2012), thereby complicating research efforts. Moreover, several virulence factors are associated with specific genetic lineages (Uruén et al., 2024). Thus, to study host-pathogen interactions and monitor bacterial behavior under certain physiological conditions, advanced experimental systems are required. For example, real-time imaging of bacterium-host interactions provides valuable insights into the spatial dynamics of *S. suis* infection and the functional roles of its virulence factors. Additionally, studies of biofilm formation help to elucidate the early stages of infection. These techniques benefit significantly from the use of fluorescently labeled bacteria, which allow direct visualization of bacterial organization, a feature closely linked to immune evasion and antibiotic tolerance (Uruén et al., 2020). Although live/dead staining techniques are frequently used, they are limited to in vitro settings and are not compatible with actively replicating bacteria. As a result, the development of fluorescent protein-expressing bacterial strains has emerged as a preferred approach.

As part of our ongoing research on *S. suis*, we aimed to produce fluorescent *S. suis* strains. Chromosomal tagging strategies were previously explored in *S. suis*, however yielded fluorescent strains that were not easily distinguished from tissue autofluorescence in fixed samples. In previous work, Kjos et al. generated a bright fluorescent *Streptococcus pneumoniae* strain by fusing the gene encoding the superfolder green fluorescent protein (sfGFP) to that of a putative histone-like protein, HlpA (Kjos et al., 2015). sfGFP is an enhanced variant of GFP with improved folding kinetics and stability under diverse chemical and physical stress conditions (Pédelacq et al., 2006). HlpA is a small, positively charged nucleoid-associated protein (Pettijohn, 1988; Dorman and Deighan, 2003). Based on this strategy, we successfully generated genetically stable and strongly fluorescent *S. suis* mutants. Here, we describe the characteristics of these strains and demonstrate their applicability in a range of in vitro and in vivo models for studying *S. suis* pathogenesis.

2. Material and methods

2.1. Bacterial strains and growth conditions

All strains used in this study are listed in Table 1. *S. suis* strains P1/7 and 10 are reference strains (Clifton-Hadley, 1984; Wisselink et al., 1999), classified as serotype 2 and sequence type (ST) 1 based on multilocus sequence typing (MLST). Disease isolates previously characterized by our group (Uruén et al., 2024) were included, which belong to serotypes 1/2, 1, 2, 9 and 14, and to genotypes ST1, ST3, ST123 and ST1643. All *S. suis* strains were grown in Todd-Hewitt broth (THB, Oxoid) or in THB with 15% of bacteriological agar (THA). When required, media were supplemented with antibiotics (100 μg/mL of spectinomycin, 25 μg/mL of chloramphenicol, or 10 μg/mL of tetracycline). For solid cultures, bacterial stocks stored at −80ºC were streaked onto THA plates and incubated overnight at 37ºC in a candle jar. For liquid cultures, colonies from THA were inoculated in 3–20 mL of THB, and incubated overnight at 37ºC. Then, overnight cultures were diluted into fresh THB to an initial optical density at 600 nm (OD_{600}) of 0.05 and incubated at 37ºC until mid-log phase (OD_{600} of 0.5). In some experiments, cultures were incubated until stationary phase (OD_{600} of ~0.8) in the presence or absence of antibiotics. Subsequently, a portion of the culture was transferred into fresh medium at an OD_{600} of 0.05 and passaged for 15 consecutive transfers. For real-time fluorescence monitoring, 1 mL of overnight THB culture was diluted to an OD_{600} of

Table 1
Bacterial strains, plasmids, and eukaryotic cell lines used in this study.

Strains, cell lines and plasmids	Relevant characteristics	Source or reference
Strains		
S. suis		
P1/7	Reference strain, serotype 2, ST1	(Clifton-Hadley, 1984)
P1/7Δ*gfp*$^+$	Derivative of P1/7 strain containing the *hlpA-sfgfp* fragment with *spec*	This study
P1/7Δ*gfp*$^+$-*tet*	Derivative of P1/7 strain containing the *hlpA-sfgfp* fragment with *tet(O)*	This study
P1/7Δ*gfp*$^+$-*cat*	Derivative of P1/7 strain containing the *hlpA-sfgfp* fragment with *cat*	This study
P1/7Δ*sly-gfp*$^+$	Derivative of P1/7 strain containing the *sly-sfgfp* fragment with *spec*	This study
P1/7Δ*eno-gfp*$^+$	Derivative of P1/7 strain containing the *eno-sfgfp* fragment with *spec*	This study
P1/7Δ*mrp-gfp*$^+$	Derivative of P1/7 strain containing the *mep-sfgfp* fragment with *spec*	This study
P1/7Δ*cps2E-F*	Derivative of P1/7 strain with the capsule locus *cpsE* and *cpsF* replaced by *spec*	(Jurado et al., 2023)
P1/7Δ*cps2E-F*Δ*gfp*$^+$	Derivative of P1/7 strain with the capsule locus replaced by *spec* and containing the *hlpA-sfgfp* fragment with *cat*	This study
10	Reference strain, serotype 2, ST1	(Wisselink et al., 1999)
10Δ*gfp*$^+$	Derivative of strain 10 containing the *hlpA-sfgfp* fragment with *spec*	This study
J28	Derivative of strain 10 with the capsule locus *cpsE* and *cpsF* replaced by *spec*	(Smith et al., 1999)
J28Δ*gfp*$^+$	Derivative of strain 10 with the capsule locus replaced by *spec* and containing the *hlpA-sfgfp* fragment with *cat*	This study
8067	Serotype 9, ST136	(Wisselink et al., 2000)
8067Δ*gfp*$^+$	Derivative of 8067 strain containing the *hlpA-sfgfp* fragment with *spec*	This study
Ss_2	Serotype 14, ST1	(Uruén et al., 2024)
Ss_2Δ*gfp*$^+$	Derivative of Ss_2 containing the *hlpA-sfgfp* fragment with *spec*	This study
Ss_45	Serotype 2, ST3	(Uruén et al., 2024)
Ss_45Δ*gfp*$^+$	Derivative of Ss_45 containing the *hlpA-sfgfp* fragment with *spec*	This study
Ss_64	Serotype 1, ST1	(Uruén et al., 2024)
Ss_64Δ*gfp*$^+$	Derivative of Ss_64 containing the *hlpA-sfgfp* fragment with *spec*	This study
Ss_72	Serotype 2, ST1	(Uruén et al., 2024)
Ss_72Δ*gfp*$^+$	Derivative of Ss_72 containing the *hlpA-sfgfp* fragment with *spec*	This study
Ss_105	Serotype ½, ST1	(Uruén et al., 2024)
Ss_105Δ*gfp*$^+$	Derivative of Ss_105 containing the *hlpA-sfgfp* fragment with *spec*	This study
Ss_106	Serotype 9, ST123	(Uruén et al., 2024)
Ss_106Δ*gfp*$^+$	Derivative of Ss_106 containing the *hlpA-sfgfp* fragment with *spec*	This study
Ss_121	Serotype 1, ST1	(Uruén et al., 2024)
Ss_121Δ*gfp*$^+$	Derivative of Ss_121 containing the *hlpA-sfgfp* fragment with *spec*	This study
Ss_134	Serotype 1, ST1643	(Uruén et al., 2024)
Ss_134Δ*gfp*$^+$	Derivative of Ss_134 containing the *hlpA-sfgfp* fragment with *spec*.	This study
E. coli		
BL21 (DE3)	Overexpression strain	Laboratory collection
BL21-HlpA	BL21 (DE3) strain with pET-16b-SsHlpA, *amp*	This study

(*continued on next page*)

Table 1 (*continued*)

Strains, cell lines and plasmids	Relevant characteristics	Source or reference
Cell lines		
BD4/21	Immortalized porcine alveolar macrophages.	(Weingartl et al., 2002)
Plasmids		
pET-16b	Plasmid for expression of N-terminally His-tagged recombinant proteins in *E. coli*	Laboratory collection
pET-16b-SsHlpA	pET-16b derivative encoding recombinant *S. suis* HlpA	This study
pCR2.1	Cloning vector	Laboratory collection
pCR2.1-P*sly-sfGFP*	pCR2.1 derivative with P*sly-sfgfp* fragment and *spec*	This study
pCR2.1-P*mrp-sfGFP*	pCR2.1 derivative with P*mrp-sfgfp* fragment and *spec*	This study
pCR2.1-P*eno-sfGFP*	pCR2.1 derivative with P*eno-sfgfp* fragment and *spec*	This study
pCR2.1-*hlpA-sfgfp*	pCR2.1 derivative with *hlpA-sfgfp* fragment and *spec*	This study
pCR2.1-*hlpA-mkate2*	pCR2.1 derivative with *hlpA-mkate2* fragment and *spec*	This study

spec: spectinomycin resistance cassette. *cat*: chloramphenicol resistance cassette. *tet*: tetracycline resistance cassette. *amp*: ampicillin resistant cassette.

0.05 in fresh THB, transferred to 24-well plates, and incubated at 37ºC in a ClarioStar Plus plate reader. OD_{600} and fluorescence intensity were measured every h after a brief 30 s shaking step. *Escherichia coli* strain BL21 (DE3) is a commercial strain used for protein production. For solid cultures, *E. coli* was grown in Luria Broth medium (LB, Sigma-Aldrich) supplemented with bacteriological agar (LBA), and incubated overnight at 37ºC. For liquid cultures, colonies collected from LBA plates were dispersed in LB and incubated at 37ºC in a shaker incubator at 100 rpm until reaching an OD_{600} of 0.8. When required, 100 μg/mL of ampicillin was added to the culture for plasmid maintenance. In addition, to induce protein production, 0.1 mM isopropyl β-D-1-thiogalactopyranoside (IPTG) was added to the liquid culture.

2.2. Genetic constructions and mutant preparation

The genetic constructs used in this study were designed based on the genome sequence of *S. suis* strain P1/7, as well as the *sfgfp* (pdb_00002b3p) and *mkate2* (DBBO8) sequences. To insert the *sfgfp* gene downstream of *sly* (SSU1231), *eno* (SSU1320) or *mrp* (SSU0706) genes, constructs were synthesized consisting of *sfgfp,* the corresponding promoter region (*sly, eno* or *mrp*), and the flanking genetic regions of each target gene. To fuse *sfgfp* to the *hlpA* gene (SSU1458), a novel construct was designed, referred to as *hlpA-sfGFP,* containing an intact *hlpA* gene without the stop codon, followed by a sequence encoding six glycine residues, an intact *sfgfp* gene, an antibiotic resistance cassette (conferring spectinomycin resistance), and 600 bp of the *hlpA* downstream region. For fusing *hlpA* to the *mkate2* gene, the *sfgfp* segment in the *hlpA-sfgfp* was replaced with *mkate2* gene. All sequences, particularly *sfgfp* and *mkate2* were codon optimized for *S. suis* (Figure S1), synthesized by BaseClear (The Netherlands), and delivered in a standard cloning vector (Table 1). All primers and particular PCR conditions are listed in Table S1 in the Supplementary material. Constructs were amplified by PCR using regular M13 primers and the Supreme NZYTaq II DNA polymerase (NZYTech) kit according to the manufacturer's instructions. PCR conditions consisted of an initial denaturation at 94ºC during 5 min, 30 cycles of 20 s at 94ºC, 30 s at 55ºC, and 68ºC during 3.5 min, and a final extension at 68ºC during 7 min. The spectinomycin resistant cassette in the *hlpA-sfgfp* fragment was replaced by chloramphenicol or tetracycline resistance cassettes by amplifying the flanking regions of the *hlpA-sfgfp* and the corresponding resistant cassettes; the three amplicons were fused together following a previously described protocol (García López et al., 2024). PCR products were separated in 1% agarose gels and visualized using Gel Green nucleic acid stain (Biotium) using a bioimaging system. DNA fragments were purified using silica columns (QIAGEN), and subsequently used to transform *S. suis* strains, as previously described (García López et al., 2024). Successful mutants were confirmed by fluorescence microscopy as described below. The *hlpA* gene from P1/7 was codon optimized and inserted in plasmid pET-16b (pET-16b-SsHlpA) by BaseClear (Leiden, The Netherlands), and introduced into *Escherichia coli* strain BL21 (DE3). Production and purification of the corresponding recombinant protein were performed following previously described standardized protocols (Arenas et al., 2015a), and the purified protein was used to raise specific mouse antiserum according to standard protocols (Arenas et al., 2015b).

2.3. Proteinase K accessibility assays

The accessibility of HlpA-sfGFP to proteinase K was assessed as previously described (Arenas et al., 2015b, 2016). Briefly, *S. suis* strains from logarithmic-phase cultures were incubated with different concentrations of proteinase K (Fermentas) at 37°C for 1 h. After incubation, the bacteria were harvested by centrifugation at 2500 x g for 10 min in a table centrifuge, and processed for whole-cell lysate preparation.

2.4. Preparation of samples, SDS-PAGE and western blotting

The preparation of subcellular fractions was performed according to our previously described methods (Arenas et al., 2015b, 2016). Shortly, for whole-cell lysates, bacteria from logarithmic liquid cultures were centrifuged (2500 x g for 10 min), and the cell pellet was resuspended in phosphate buffered saline (7.7 mM Na_2HPO_4, 2.3 mM NaH_2PO_4, 145.5 mM NaCl, pH=7.35) and adjusted to an OD_{600} of 10 or 1 for *S. suis* and *E. coli*, respectively. For cell envelope preparation, bacteria from THB cultures were harvested by centrifugation (2500 x g for 10 min), and the cell pellet was resuspended in 2 mM Tris-HCl buffer, sonicated (3 bursts of 1 min at 250 W with a 30 s cooling period), and the resulting suspension was centrifuged (2500 x g for 10 min) to remove cell debris. The cell envelopes in the spent supernatant were harvested by ultracentrifugation (20,000 x g during 3 h at 4ºC). The resulting pellet was resuspended in Tris-HCl buffer (2 mM Tris Base, pH=7.4) with constant shaking at 4ºC. For supernatant preparations, the resulting media from ultracentrifugation was mixed with 10% (w/v) trichloroacetic acid for 30 min on ice to precipitate the proteins. The proteins were then harvested by centrifugation (16000 x g for 10 min), and the resulting pellet was washed with ice-cold acetone, air dried and resuspended in distilled H_2O. All samples (whole-cell lysates, supernatants and cell envelopes) were diluted in double-strength sample buffer containing 8% SDS and 2% β-mercaptoethanol and heated at 100ºC during 10 min. Then, the proteins were separated in 12% polyacrylamide gels at 200 V during 45 min. The gels were next incubated with Coomassie Brilliant Blue G250 (ITW Reagents) to stain the proteins, or subjected to 100 V during 1 h to transfer the proteins to nitrocellulose membranes (Thermo Fisher). Membranes were blocked with PBS containing 0.1% of Tween 20 and 3% of nonfat dry milk (Sigma-Aldrich) during 1 h at room temperature. Then, the membranes were washed twice with PBS and incubated with commercial anti-GFP monoclonal antisera (Sigma-Aldrich), polyclonal anti-GlnP sera directed against the product of the SSU1675 gene, which is part of a putative ABC transporter functioning as a permease (laboratory collection) or anti-HlpA sera (this work) at working dilutions in PBS containing 0.1% of tween 20 (Sigma-Aldrich) and 0.5% of nonfat dry milk. After washing, the membranes were incubated with a horseradish peroxidase-conjugated goat anti-mouse IgG (Biosource International) during 1 h at room temperature, washed twice with PBS, and revealed with the Pierce ECL substrate (BioRad). Proteins were visualized using an imaging system (iBright 1500, Invitrogen).

2.5. Flow cytometry

Flow cytometry assays were performed following a modification of our previous methods (Arenas et al., 2008). Briefly, bacteria from exponential cultures were fixed with 1% formaldehyde for 1 h at 37 ºC, collected by centrifugation, and resuspended in PBS at an OD_{600} of 0.3. Fluorescence was measured using an Attune CytPix Flow Cytometer (Invitrogen). Data were plotted using FloJo v11 software.

2.6. Biofilm formation

S. suis biofilms were formed as previously described (Jurado et al., 2023). Briefly, bacteria from exponential-phase cultures were adjusted to an OD_{600} of 1, placed in 24-well plates (Techno Plastic Products), and incubated during 24 h. After incubation, the supernatant was removed, and each biofilm was washed with deionized water. The biomass was stained with crystal violet and quantified as previously described (Arenas et al., 2015b, 2016).

2.7. Mice infections

A *S. suis* nasal mucosal colonization model described by Seitz et al (Seitz et al., 2012) was adapted here. All animal experiments described here were approved by the Animal Welfare Committee of CITA (permit number 2023_01) and conducted in accordance with its guidelines and policies. Five-week-old CD-1 mice were provided by Janvier Lab (France). Animals were housed in level II facilities at CITA, and feeding was managed by authorized personnel. Mice were randomly assigned into eight groups of six female mice. After a one-week adaptation period, the animals were anesthetized using isoflurane (Isoflo, Zoetis), and 12.5 µl of 1% acetic acid was added to each nostril as pre-treatment. One h later, after a controlled recovery phase and further anesthesia, mice were intranasally inoculated with 5×10^8 CFU. Health, behavior, and weight were monitored every eight h to track clinical signs of streptococcal infection (depression, swollen eyes, rough hair coat, prostration, and lethargy). After three, seven and fourteen days of infection, animals were euthanized using CO_2, followed by cervical dislocation. Nostrils and internal organs (spleen, brain, lungs, heart) were extracted, weighed, and homogenized in a stomacher (Seward Limited) using sterile bags. Then, the number of viable bacteria was determined by serial dilution of samples and plating on THA supplemented with spectinomycin.

2.8. Eukaryotic cell cultures and infection assays

The porcine macrophage cell line 3D4/21 was cultured in Roswell Park Memorial Institute medium (RPMI) 1640 medium and supplemented with GlutMAX, 10% non-heat-inactivated fetal calf serum (FCS) and 1% commercial antibiotic-antimycotic solution. All cell culture components were provided by PAA laboratories GmbH (Pasching, Australia). 3D4/21 cells were grown in 25 cm^2 tissue-culture flasks (Nunc) under standard conditions of 37°C in a humidified atmosphere with 5% CO_2, until reaching approximately 80% confluence. For bacterial association assays, cells from passages 4–25 were seeded in 24-well (3D4/21), with sterile glass coverslips, two days before infection. One day before infection, the culture medium was replaced with fresh medium lacking antibiotics. Macrophages were stimulated with 1 ng/mL of *E. coli* Lipopolysaccharide (Sigma) for 24 h to enhance phagocytic activity. Bacteria in the logarithmic growth phase were harvested by centrifugation at 1500 x *g* during 10 min, resuspended in RPMI, and added to macrophage cultures at a multiplicity of infection (MOI) of 100. After 3 h of infection, cells were washed three times with Dulbecco's Phosphate-Buffered Saline (DPBS) to remove non-adherent bacteria. To lyse the macrophages, 500 µl of cold sterile water was added to each well. The lysate was serially diluted and plated on THA for colony-forming units (CFU) counting.

2.9. Sample preparation, microscopy and image analyses

S. suis strains from logarithmic-phase cultures were placed on coverslips, dried for fixation, and visualized using an Olympus CX41RF fluorescence microscope (Olympus Optical Co.). For the microscopic examination of biofilms, biofilms were formed in 24-well plates containing round glass coverslips, washed, and fixed with PBS containing 4% formaldehyde for 1 h. The biofilms were subsequently washed and imaged using a Zeiss LSM 880 confocal laser scanning microscope equipped with a Plan-Apochromat 40x/0.85 oil objective (Zeiss Microscopy). Image Z-stacks were acquired at 0.4 µm intervals and used to study biofilm architecture using COMSTAT software (Heydorn et al., 2000; Wrobel et al., 2020). For visualization of bacteria in infected tissues, the brain, heart, lungs and spleen were collected from euthanized infected mice. The organs were immersed in PBS containing 4% of formaldehyde for 1 h, embedded in OCT (Optimal Cutting Temperature) compound (Thermo Fisher), and frozen at −80 °C. Tissue sections were cut using a cryotome and visualized under both fluorescence and brightfield conditions using a Leica AF6000 LX microscope, or under optical microscopy after staining with hematoxylin and eosin. For the analysis of cell-associated bacteria in infected cultured cells, infected macrophages were washed with DPBS and incubated at 37ºC during 1 h with primary monoclonal antibody 74–22–15 (Novus Biologicals), which specifically binds porcine monocytes and/or granulocytes, diluted in DPBS with 10% bovine serum albumin. After three washes with DPBS, cells were incubated during 1 h at 37ºC with a goat anti-mouse IgG secondary antibody conjugated to Alexa Fluor 594 (Thermo Fisher) diluted in DPBS. Then cells were washed three times with DPBS and fixed in 2% formaldehyde in DPBS. Infected cell preparations were observed under a fluorescence microscope (Zeiss Axio Observer) with an AxioCam MRm camera. For all microscopy-based experiments, fluorescence intensity measurements were normalized relative to negative controls (tissue autofluorescence or non-fluorescent bacteria).

2.10. Statistical analysis

For statistical comparisons, data from at least three independent experiments, each performed in duplicate, were used. Statistical analyses were performed using the non-parametric unpaired Mann–Whitney *U* test, except for flow cytometry data, which were analyzed using a two-way repeated-measures ANOVA with Geisser–Greenhouse correction followed by Tukey's multiple comparisons test. All analyses were performed using GraphPad Prism version 6. Statistical significance between groups was considered at $P < 0.05$ or $P < 0.001$.

3. Results

3.1. Engineering fluorescent S. suis strains

To engineer fluorescent *S. suis,* we initially introduced sfGFP- and far-red fluorescent mKate2-encoding genes (*sfgfp* and *mkate2*, respectively) into the *S. suis* chromosome to create stable fluorescent strains. To ensure sufficient protein expression, we decided to place these genes downstream of the Suilysin-encoding gene (*sly*), following, in part, the strategy described by Chen et al. (2012). (Figure S2). Codon-optimized *sfgfp* and *mkate2*, along with a spectinomycin resistance cassette and flanking regions, were inserted into the *S. suis* chromosome downstream of the *sly* gene in the strain 10. The resulting transformants exhibited limited fluorescence under fluorescence microscopy (data not shown). Then, we placed *sfgfp* behind Murein-Released Protein (*mrp*) and Enolase (*eno*) encoding genes (Figure S2), but this strategy also failed to enhance fluorescence emission (data not shown). To improve it, we fused *sfgfp* and *mkate2* genes to the *hlpA* gene, which encodes the histone-like protein HlpA. These fusion constructs were designed to integrate the target genes into the chromosome (Fig. 1A), following a

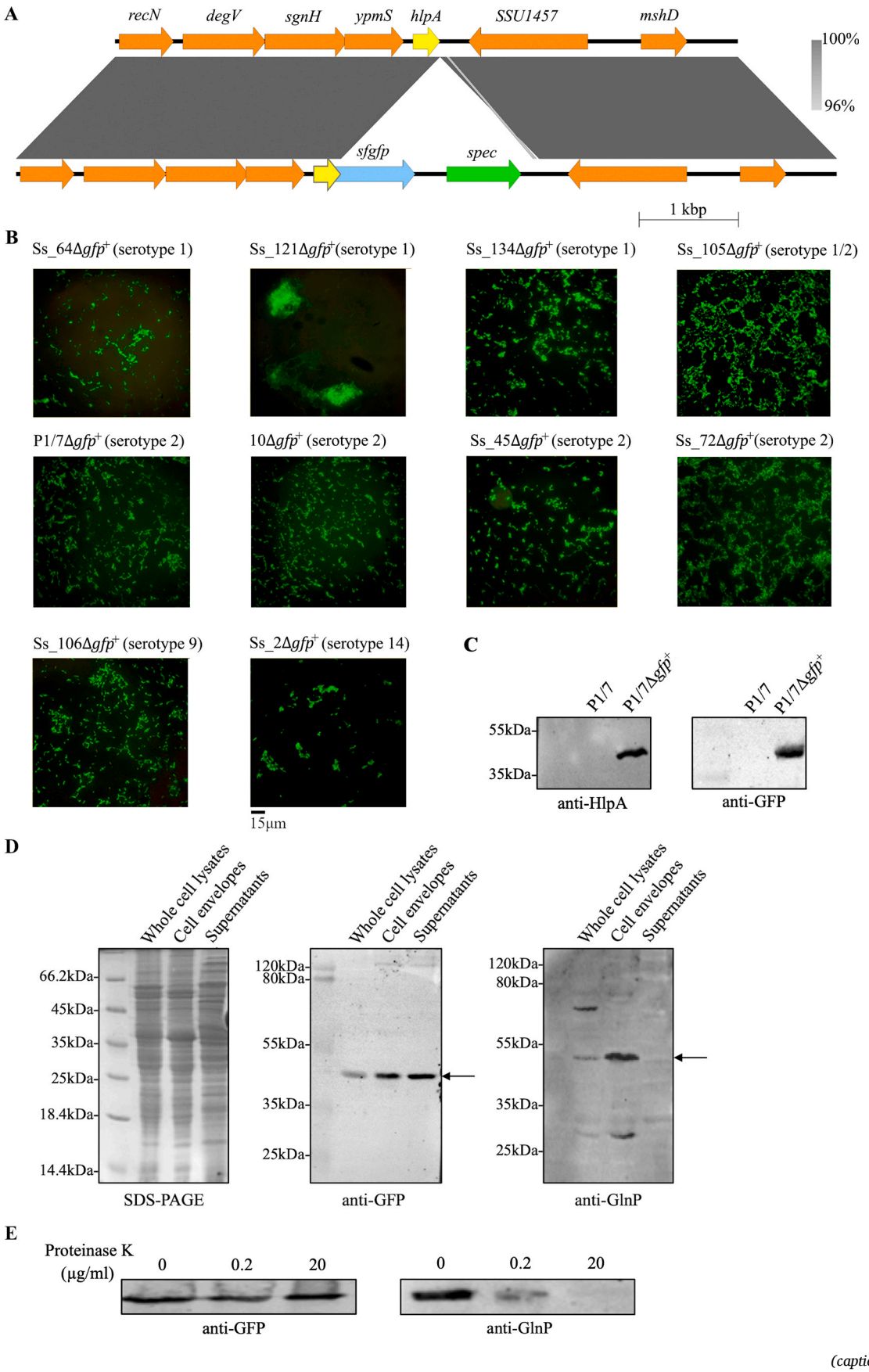

(caption on next page)

Fig. 1. Generation, characterization and localization of HlpA-sfGFP fluorescent *S. suis* strains.(A) Schematic representation of the genetic context of the *hlpA* gene in the P1/7 strain and its fluorescent mutant derivative containing the *hlpA-sfgfp* fusion. (B) Fluorescence microscopy images of *S. suis* strains from various serotypes harboring *hlpA-sfgfp* fusions. (C) Western blot analyses of whole-cell lysates from strains P1/7 and P1/7Δ*gfp*$^+$ probed with a polyclonal antiserum against HlpA and a monoclonal antiserum against GFP. (D) SDS-PAGE and Coomassie Brilliant Blue G250 staining of whole-cell lysates, cell envelope fractions and supernatant preparations from P1/7Δ*gfp*$^+$ (left panel). Western blot analyses were performed with a monoclonal antiserum against GFP (middle panel) and a polyclonal antiserum against a putative glutamine permease (right panel). Arrows indicate the HlpA-sfGFP fusion protein and the membrane protein GlnP. (E) Surface accessibility of HlpA-sfGFP assessed by treating intact cells of strain P1/7Δ*gfp*$^+$ with increasing concentrations of proteinase K, followed by Western blot detection of protein degradation.

previously successful strategy for generating fluorescent *S. pneumoniae* (Kjos et al., 2015). The *hlpA-sfgfp* and *hlpA-mkate2* fusion constructs were used to transform pathogenic *S. suis* reference strains P1/7 and 10 of serotype 2, and clinical isolates Ss_45 and Ss_72 of serotype 2, Ss_64, Ss_121 and Ss_134 of serotype 1, 8067 and Ss_106 of serotype 9, Ss_2 of serotype 14, and Ss_105 of serotype 1/2. Fluorescent transformants were successfully generated for all strains with the *hlpA-sfgfp* fusion (Fig. 1**B**), but we did not obtain transformants with the *hlpA-mkate2* fusion. Visualization of fluorescent strains under the microscope revealed a different level of aggregation, including very aggregative strains such as Ss_121, strains with low size aggregates without interaction (Ss_72, Ss_134), strains with aggregates that interacted with each other (Ss_105), or low aggregative strains (Ss_64, Ss_45). A comparison of growth curves for representative strains 10, P1/7, and 8067 with their fluorescent derivatives revealed no growth defects (Figure S3A), suggesting that sfGFP production did not negatively impact cell viability as earlier shown for *S. pneumoniae*. The fluorescence emission was recorded for P1/7Δ*gfp*$^+$ and P1/7. In contrast to P1/7, analysis of P1/7Δ*gfp*$^+$ growth revealed a progressive increase in fluorescence intensity that correlated with the OD_{600} (compare Figure S3A and S3B). This suggests that our fluorescent mutants can be used for growth monitoring. Furthermore, fluorescent mutants were generated using different antibiotic-resistant markers (Table 1), all of which exhibited similar fluorescence intensity levels, demonstrating the versatility of the system.

3.2. Analysis of HlpA-sfGFP fusion

To investigate the production and integrity of the HlpA-sfGFP fusion protein, HlpA was produced in *E. coli* as a recombinant protein, purified using Ni-NTA agarose beads (Figure S4**)**, and used to raise specific antibodies. Western blotting analyses with anti-HlpA antibodies detected the recombinant HlpA protein, but these antibodies hardly reacted with HlpA in whole-cell lysates of P1/7 while a band of ~37 kDa was detected in whole-cell lysates of P1/7Δ*gfp*$^+$ (Fig. 1C). This band was also detected with anti-GFP antibodies (Fig. 1C) and corresponds to the expected size of the HlpA-sfGFP fusion protein (37 kDa). No degradation products were detected with either antibody. HlpA is a putative nucleoid-binding protein in *Streptococcus* spp., likely associated with the chromosome. As a result, HlpA-sfGFP is expected to localize intracellularly. To verify this, we examined the subcellular localization of HlpA-sfGFP by analyzing its presence in whole-cell lysates, cell envelopes and concentrated supernatants of P1/7Δ*gfp*$^+$. SDS-PAGE analysis of the three preparations revealed different protein profiles for each of the subcellular fractions (Fig. 1D). The samples were then probed with specific antibodies against a putative membrane protein encoded by SSU1675, called GlnP. Mature GlnP has a predicted molecular size of 54 kDa. The antibody directed against GlnP detected a band with the expected molecular size in whole-cell lysates, which was more abundant in cell envelope preparations but absent in supernatants (Fig. 1D). This is in full agreement with the localization of GlnP in the membrane and indicates that that the preparation of the samples is correct. In contrast, anti-GFP and anti-HlpA antibodies detected HlpA-sfGFP in whole-cell lysates, cell envelopes, and supernatant preparations with no differences in its molecular size (Fig. 1D right panels). To determine whether sfGFP was surface-exposed, we conducted proteinase K susceptibility assays on intact bacteria. This protease successfully cleaved GlnP, which contains about 270 surface-exposed amino acids that are targeted by the anti-GlnP antibodies. In remarkable contrast, proteinase K did not degrade HlpA-sfGFP (Fig. 1E). Together, these analyses indicate that HlpA-sfGFP is located intracellularly but is also released to the milieu while HlpA and sfGFP remain stably fused.

3.3. Fluorescence stability analysis

To evaluate the stability of the fluorescent mutant, strain P1/7 and its fluorescent derivative were cultured in THB, the latter with and without spectinomycin, until reaching an OD_{600} of ~ 0.8. These cultures were then serially passaged 15 times. At passages 1, 5, 10 and 15, bacterial samples were collected, inactivated with formaldehyde, and analyzed for fluorescence intensity using flow cytometry. Both strains exhibited comparable forward and side scatter profiles (Fig. 2A), but clearly significant differences were detected between P1/7 and the fluorescence derivative, indicating that our fluorescence mutants are also nicely distinguishable by FACS from non-fluorescent strains (Fig. 2B). Remarkably, fluorescence intensity remained consistent across all tested passages independently of the presence or absence of spectinomycin in the culture medium, indicating that long-term fluorescence retention does not depend on antibiotic selection pressure (Fig. 2B). Also, no decrease in fluorescence was detected across passages for the fluorescent mutant. Thus, the fluorescence is nicely preserved.

3.4. Biofilm formation studies

S. suis is known to form biofilms on abiotic surface which can be monitored by fluorescence microscopy. To investigate the potential of our fluorescent strains for studying biofilm formation on abiotic surfaces, we first evaluated the biofilm-forming capacity of the wild-type strains P1/7 and 10 and their corresponding fluorescent derivatives. Biofilms were formed on polystyrene plates and quantified using crystal violet staining at 24 h and 48 h. No significant differences were detected between wild-type and fluorescent mutant strains (Figure S5), suggesting that the GFP production did not affect biofilm formation capacity. We then compared the biofilm-forming capacity of several *S. suis* strains and their fluorescent derivatives. First, the biofilm biomass of the parental strains was quantified using conventional crystal violet staining. Strain Ss_121 exhibited a five-fold increase in biofilm formation compared to strains P1/7, 10, Ss_106, and Ss_134 (Fig. 3A). Biofilms of the fluorescent mutant derivatives were grown on glass and visualized after 24 h using confocal microscopy (Fig. 3B). The results were consistent with those observed in the parental strains, showing a similar capacity to produce biofilms. Biofilms formed by P1/7Δ*gfp*$^+$ and 10Δ*gfp*$^+$ consisted of small microcolonies interspersed with single cells. Similarly sized microcolonies were observed in biofilms of Ss_106Δ*gfp*$^+$, although these aggregates were fewer and less interconnected than those produced by P1/7Δ*gfp*$^+$ and 10Δ*gfp*$^+$. In contrast, biofilms of Ss_134Δ*gfp*$^+$ consisted of smaller aggregates and scattered single cells, producing a less structured architecture than those of P1/7Δ*gfp*$^+$, 10Δ*gfp*$^+$, and Ss_134Δ*gfp*$^+$. Notably, Ss_121Δ*gfp*$^+$ produced biofilms composed of large and highly interconnected aggregates that covered more than 80% of the substratum. These observations are consistent with the results from the crystal violet staining assay. To further analyze the structural properties of the biofilms, we used the COMSTAT software. Ss_121Δ*gfp*$^+$ biofilms exhibited the highest values for biomass production, mean biomass thickness, area thickness, and surface-to-

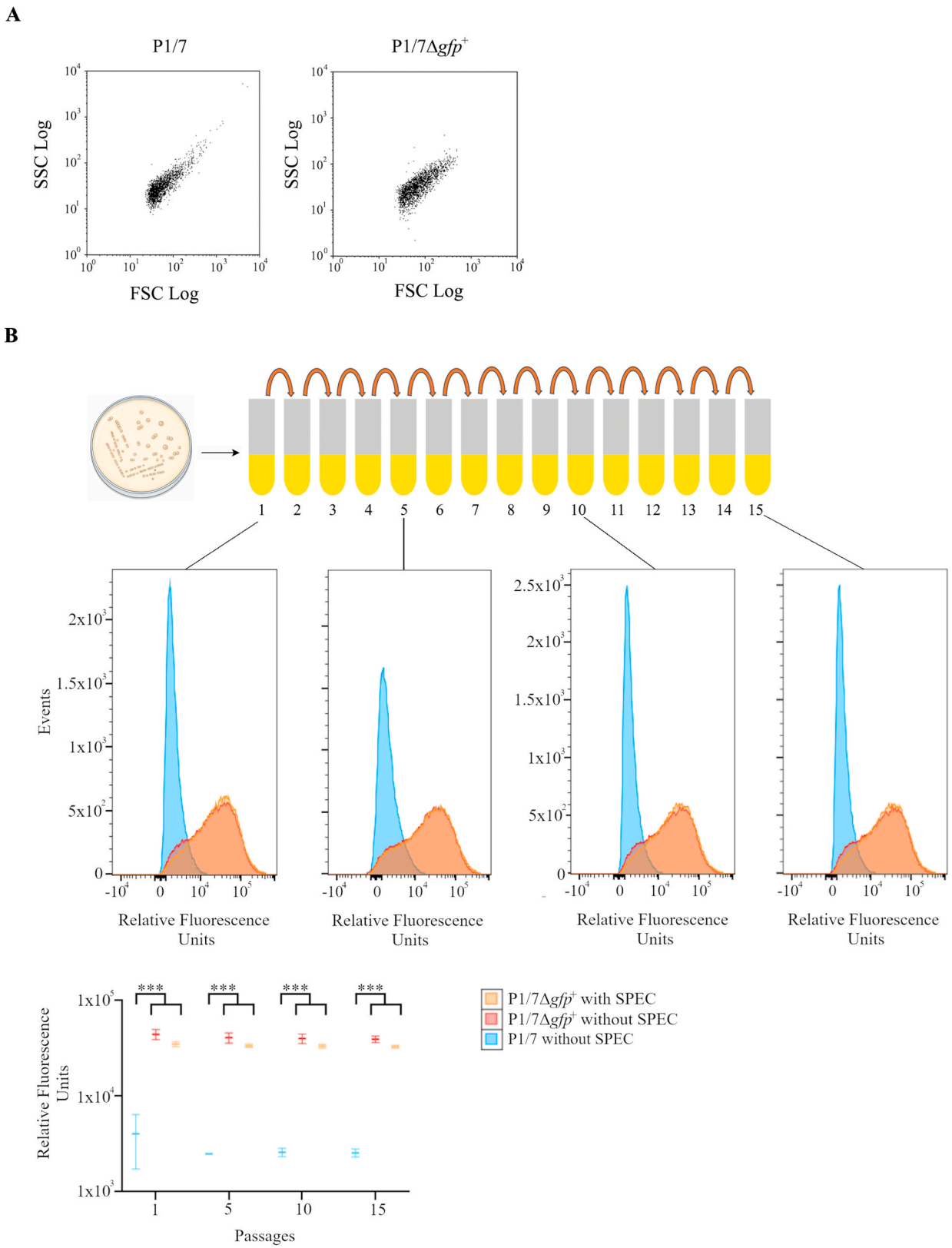

Fig. 2. Detection and stability of the fluorescence emission across bacterial generations. (A) FSC and SSC analysis of populations of P1/7 and P1/7Δ*gfp*$^{+}$. (B) Schematic representation of the experimental design used to evaluate fluorescence stability. P1/7Δ*gfp*$^{+}$, which carries a spectinomycin resistant marker, was grown in Todd-Hewitt broth with or without spectinomycin, and subcultured for 15 consecutive passages. Flow cytometry analysis of formalin-killed bacterial populations obtained after 1, 5, 10 and 15 passages are shown in the histograms. Graphical representation of the mean ± standard deviation of three biological replicates of fluorescence intensity of each population at every passage. Statistical difference is indicated by three asterisks ($P < 0.001$).

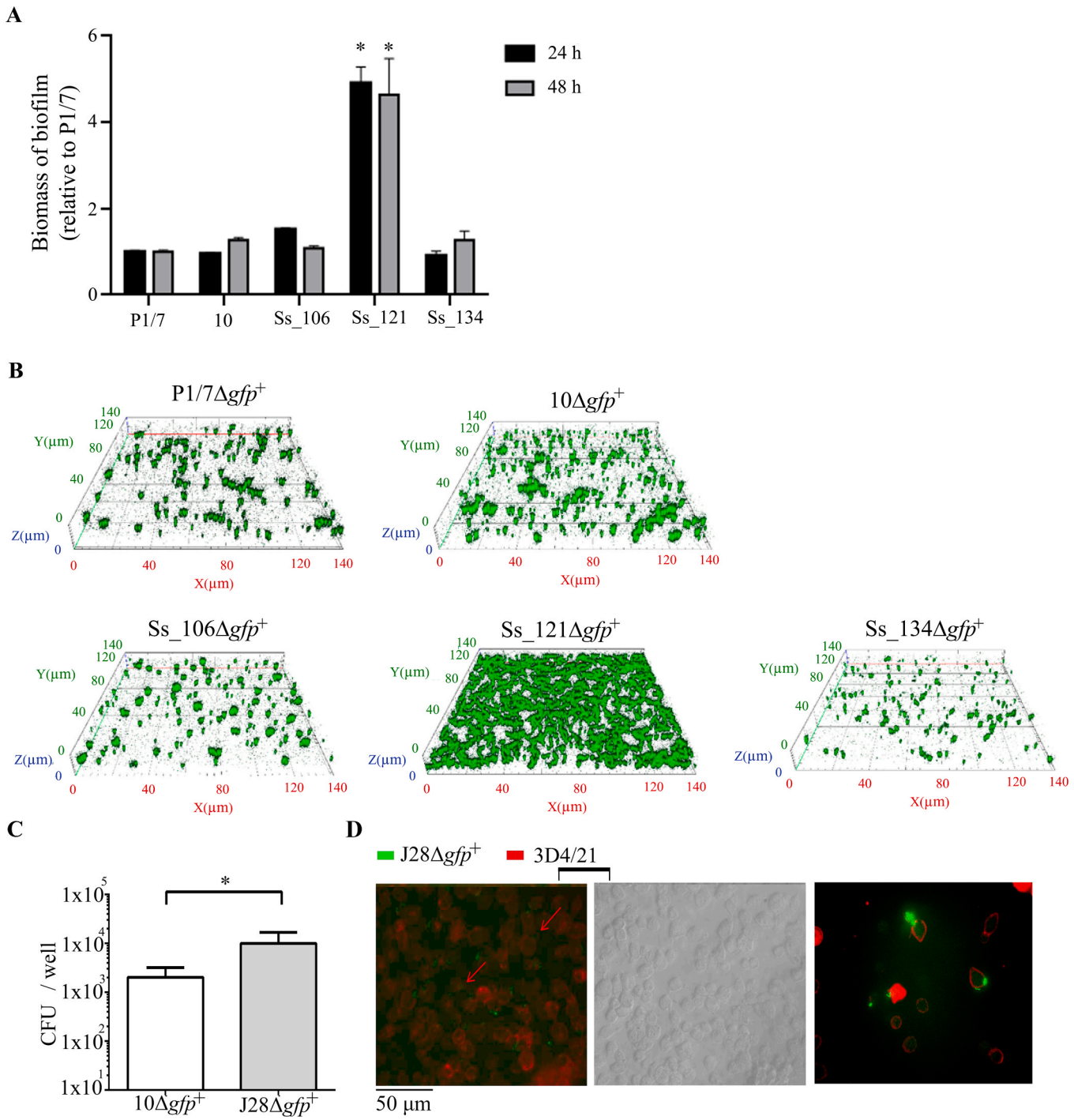

Fig. 3. Analysis of the interaction between the new fluorescent mutants and biotic and abiotic surfaces. (A) Quantification of biofilm biomass using crystal violet staining. No differences in biofilm formation capacity were detected between wild-type and fluorescence derivatives (Fig. S4). (B) Confocal microscopy analysis of 24 h biofilms. (C) Quantification of cell-associated bacteria in infected macrophage cultures. The mean and standard variation from at least three independent experiments with two technical replicates are shown. Statistical difference is indicated with one asterisk ($P < 0.05$). (D) Fluorescence microscopy images showing strain J28Δ*gfp*$^+$ localized within red-stained macrophages (left and middle panels) and extended-focus (right) of the adhesion of green fluorescent bacteria to red-stained macrophages. Red arrows indicate presumably intracellular bacteria, while blue arrows indicate presumably located on the cell surface.

volume ratio. However, they displayed a lower roughness coefficient compared to the other strains (Figure S6). In contrast, Ss_106Δ*gfp*$^+$ and Ss134Δ*gfp*$^+$ biofilms showed increased roughness and reduced biomass thickness relative to P1/7Δ*gfp*$^+$ and 10Δ*gfp*$^+$ (Figure S6). Together, these results demonstrate that *S. suis* forms biofilms with distinct architectures and confirm that our fluorescent construct allows a detailed biofilm analysis of *S. suis* on abiotic surfaces.

3.5. Eukaryotic-bacterial interactions

Eukaryotic-bacterial interaction assays are widely used to evaluate the activity of virulence factors, including interactions with macrophages, epithelial, and endothelial cells. To further demonstrate that our bright fluorescent mutants could be useful for visualizing interactions with eukaryotic cells, we infected a porcine macrophage cell line with fluorescent strain 10. Because the bacterial capsule is a relevant factor

influencing adhesion by masking adhesins and inhibiting phagocytosis, we included its corresponding capsule-deficient mutant in our assays. The porcine alveolar macrophages cell line 3D4/21 was infected with both strains, and the number of cell-associated bacteria was quantified after 3 h. Indeed, the unencapsulated mutant derivative J28Δ*gfp*$^+$ exhibited significantly higher levels of adhesion compared to the parental strain 10Δ*gfp*$^+$ (Fig. 3C). To visualize these interactions, infected macrophages were stained with specific antibodies emitting red fluorescence, fixed, and examined under a fluorescence microscope. Indeed, aggregates of fluorescent J28Δ*gfp*$^+$ were observed on the macrophage surface, with some bacteria internalized (Fig. 3D). These experiments confirm that the capsule significantly limits bacterial adhesion and emphasize the utility of our fluorescent mutants for studying host-pathogen interactions at the cellular level.

3.6. Testing fluorescent mutants in mice infection models

To evaluate the utility of our fluorescent mutants in studying host-pathogen interactions, we employed a murine intranasal infection model. Murine models are widely used to investigate *S. suis* infections, particularly for analyzing virulence factors, assessing vaccine efficacy, or testing novel antimicrobial treatments (Gilmer et al., 2017). Our goal was to evaluate whether the fluorescent mutants could be used to analyze bacterial virulence. The capsule is a well-known virulence factor in *S. suis* (Smith et al., 1999). Thus, we created a double mutant lacking the capsule and expressing fluorescence, called P1/7Δ*cps2E-F*Δ*gfp*$^+$ (Table 1). This mutant showed no growth differences compared to the non-fluorescent capsule-deficient derivative P1/7Δ*cps2E-F* (data not shown). Mice were then intranasally infected with 10^8 CFU of either fluorescent mutant. Two days post-infection (dpi), the animals showed clinical signs of infection, including lethargy, weight loss, and nasal discharge. At 3, 7 and 14 dpi, the animals were euthanized, and their organs were collected for bacteriological or histological analysis. Examination of nasal tissue at 3 dpi revealed an average of around 10^7 CFU of P1/7Δ*gfp*$^+$ per g, indicating successful colonization. At 7 and 14 dpi, the average bacterial counts had decreased by approximately 7-fold and more than 100-fold, respectively (Fig. 4A). In spleen and heart tissues, average bacterial loads for P1/7Δ*gfp*$^+$ were around 10^3 - 10^4 CFU/g at 3 and 7 dpi, but dropped considerably by 14 dpi (Fig. 4B, C). Notably, P1/7Δ*gfp*$^+$ was recovered from the brain of several animals at both 3 and 7 dpi (Fig. 4D). Finally, P1/7Δ*gfp*$^+$ was detected in the lungs at 3 and 7 dpi but not at 14 dpi (Fig. 4E). This suggests that P1/7Δ*gfp*$^+$ reached the bloodstream and initially survived enough to colonize internal organs and cross the blood-brain barrier before being cleared by the host immune response. Comparison of bacterial loads of P1/7Δ*gfp*$^+$ at 7 dpi in different organs with those derived from our recent experiments (García et al., 2026) using the same infection model and dose revealed no significant differences compared with P1/7 with the exception of heart tissues, where P1/7Δ*gfp*$^+$ was detected in four of six mice, in contrast to P1/7 which was not detected at all (Figure S7); however, the large interindividual variability did not prevented significant differences. These comparisons suggest that P1/7Δ*gfp*$^+$ did not lose virulence compared to the wild-type. In contrast, nasal bacterial loads of P1/7Δ*cps2E-F*Δ*gfp*$^+$ were between 100- and 1000-fold lower than P1/7Δ*gfp*$^+$ at all tested times (Fig. 4A). The unencapsulated mutant was isolated from the brain of only one mouse (Fig. 4D) and was not isolated from spleen, heart or lungs (Fig. 4B, C, E), suggesting its inability to disseminate or survive in the bloodstream. Representative infected tissues were fixed, frozen, used to make histological sections using a cryostat, and visualized by microscopy. Hematoxylin-eosin-stained cryosections showed signs of inflammation, including mixed inflammatory cell infiltration in the spleen and chronic inflammatory cells in the heart (Fig. 4F), thus confirming the virulence of the fluorescent background strain. To visualize fluorescent bacteria in mouse tissues, cryosections were examined under epifluorescence and confocal microscopy. Fluorescent bacteria were detected in all P1/7Δ*gfp*$^+$-infected tissues mainly forming bacterial aggregates (see representative images in Fig. 4G). Together, our findings demonstrate that P1/7Δ*gfp*$^+$ retains its pathogenic potential and successfully establishes streptococcal infection in a murine model. In contrast, the non-capsular mutant derivative exhibited a reduced capacity to infect and disseminate within the host. Moreover, the fluorescent bacteria can be visualized in host tissues where its fluorescence intensity was considerably higher than tissue autofluorescence as earlier reported for *S. pneumoniae* (Kjos et al., 2015).

4. Discussion

Fluorescently labeled mutants have been developed for several *Streptococcus* species (Aymanns et al., 2011; Aspiras et al., 2000; Mu et al., 2021; Lautenschläger et al., 2024; Odo et al., 2024). In *S. suis*, early work by Lun and Willson (2004) described the construction of fluorescent strains SX332 and SX932, both of serotype 2, by introducing the GFP gene under the control of the *sly* promoter in a plasmid derived from pShut plasmid (Lun and Willson, 2004). These mutants exhibited detectable fluorescence using epifluorescence microscopy and flow cytometry, and the signal intensity was sufficient to distinguish fluorescent *S. suis* from pig tonsil tissue in experimentally infected animals. While plasmid-based systems offer a versatile platform for engineering fluorescent strains, they present notable limitations, including potential instability under varying environmental conditions and the risk of horizontal gene transfer to other microorganisms. Unfortunately, the long-term stability of fluorescence in the Lun and Willson study was not assessed (Lun and Willson, 2004). A more robust approach involves chromosomal integration of fluorescent markers. In a subsequent study, Chen et al. generated fluorescent mutants of *S. suis* strain HA9801 (serotype 2) by integrating the *egfp* gene, a gene encoding enhanced GFP, into the chromosome downstream of the *sly* gene (Chen et al., 2012). However, because *sly* is not conserved across all *S. suis* strains, this strategy lacks universal applicability. The resulting fluorescence mutants were biochemically stable over multiple passages. Moreover, the fluorescent mutant exhibited virulence comparable to the wild-type strain in mouse infection assays, indicating that the genetic modification did not attenuate pathogenicity. However, the fluorescence signal was insufficient to distinguish the bacteria from tissue autofluorescence in certain infected organs.

In our study, we also opted for chromosomal integration of the fluorescent marker. In contrast to the approach of Chen et al., we used a sfGFP that folds rapidly and is more resistant to stress conditions than eGFP. Initially, we inserted the promoter of *sly*, *mrp* and *epf* upstream *sfgfp* and placed downstream of the cited loci, as they are highly produced virulence factors. We deliberately avoided fusing *sfgfp* to these genes, to prevent potential interference with virulence-related genes function. The resulting mutants produced weak fluorescence. Notably, earlier reports have shown relatively low expression of sly (Xu et al., 2021) and mrp (Zhang et al., 2014) in the P1/7 strain compared to other highly virulent *S. suis* strains. As authors used different strains, this may explain the discrepancies with our results. Alternatively, as these genes code for virulence factors, they may be downregulated *in vitro*. Our previous work analyzing the transcriptome of *S. suis* strain 10 recovered from infected animals versus grown in THB showed that the expression of the genes coding for enolase and MRP were not upregulated *in vivo* (Arenas et al., 2019). However, high expression levels of the *sly* gene were detected in tissue and blood associated bacteria from infected animals as compared with THB (Arenas et al., 2019). Nevertheless, beyond the biological explanations that may account for the weak fluorescence signal in the reference strains used in this work, these constructs did not produce strains suitable for our intended applications and therefore we explored alternative strategies.

Inspired by the work of Kjos et al. (2015), who achieved strong fluorescence in *S. pneumoniae* by fusing sfGFP to the nucleoid-binding protein HlpA, we adapted this approach for *S. suis*. This strategy

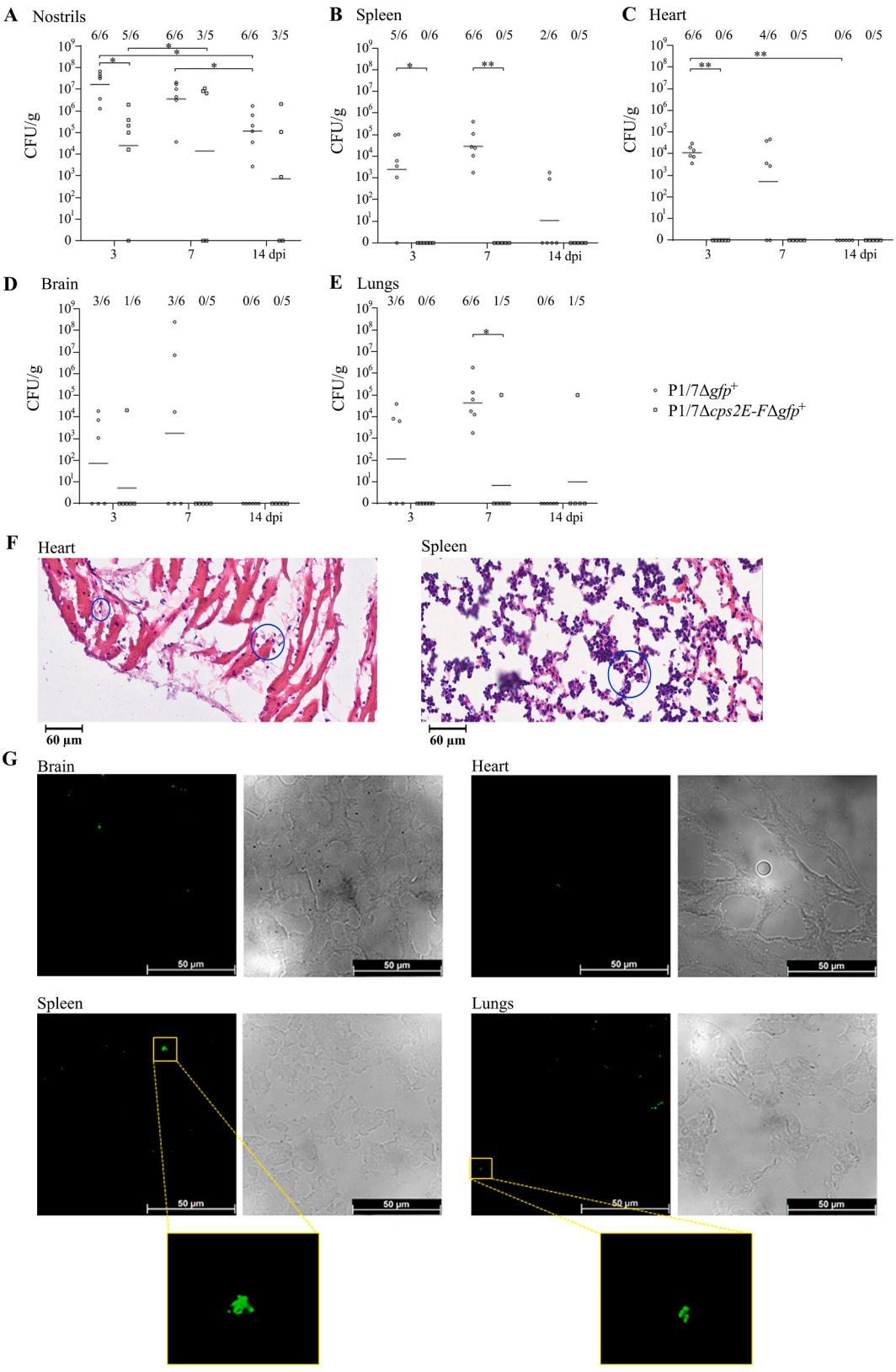

Fig. 4. Analysis of the virulence of fluorescent *S. suis* mutants in a murine infection model. Mice were intranasally infected with strain P1/7Δ*gfp*$^{+}$ and its capsule mutant derivative P1/7Δ*cps2E-F*Δ*gfp*$^{+}$. At 3,7 and 14 days post-infection (dpi), animals were sacrificed, and bacterial loads in various internal organs were quantified by colony forming units (CFUs) counts per gram of tissue (CFU/g) in (A) nostrils, (B) spleen, (C) heart, (D) brain, and (E) lung tissues. (F) Cryosections of tissues from P1/7Δ*gfp*$^{+}$- infected mice were stained with hematoxylin and eosin showing inflammatory cells (circled). (G) P1/7Δ*gfp*$^{+}$-infected tissues were examined by fluorescence microscopy to visualize the fluorescent bacteria. Statistical significance at $P < 0.05$ and $P < 0.001$ is indicated with one or two asterisks, respectively.

enabled the generation of brightly fluorescent strains across multiple *S. suis* serotypes and genetic lineages (Fig. 1B). The system is compatible with different antibiotic resistance markers (spectinomycin, tetracycline, and chloramphenicol), which facilitates the creation of additional mutations. The resulting strains exhibited sufficient fluorescence intensity for a wide range of applications, including real-time fluorescence-based growth monitoring (Figure S3), flow cytometry (Fig. 2), and diverse fluorescence microscopy techniques (Figs. 1, 3, 4). The strong fluorescence signal enabled detailed analyses of the variability of *S. suis* biofilm architecture (Figs. 3A-B, S6), interactions with eukaryotic cells (Fig. 3C-D), and visualization of bacteria within tissues from experimentally infected animals (Fig. 4). Importantly, the fluorescent strains retained virulence in mouse infection models (Fig. 4A-E), with similar bacterial loads than P1/7 7 dpi (Figure S7), and fluorescence expression remained stable over at least 15 serial passages (Fig. 2), supporting their suitability for long-term experiments. In contrast to the findings of Kjos et al., we were unable to produce red fluorescent HlpA fusion using the mKate2 protein, possibly due to its cytotoxic effect in *S. suis*.

Our western blot analysis revealed the integrity of HlpA-sfGFP fusion protein (Fig. 1D), with no detectable degradation products, in contrast to previous observations in *S. pneumoniae* where some degradation products were observed (Kjos et al., 2015). This probably explains the high fluorescence intensity and stability detected in our strains. Kjos et al. proposed that fusion of HlpA with sfGFP likely enhances fluorescence by localizing the protein at the chromosome, thereby reducing the diffusion of the fluorescence signal. Although HlpA was initially assumed to localize in the nucleoid, proteomic analysis has identified HlpA homologous on the cell surface in certain species, such as *S. pyogenes* (Severin et al., 2007) or *Mycobacterium smegmatis* (Katsube et al., 2007). HlpA lacks classical secretion signals or membrane-anchoring motifs, but it may bind lipoteichoic acids located in the cell wall of Gram-positive bacteria (Stinson et al., 1998). This may explain its association with the bacterial cell surface in some species. In *Helicobacter pylori,* HlpA homologous have even been detected in the extracellular medium (Kim et al., 2002), although the mechanism by which HlpA crosses the membrane remains enigmatic. Our findings partially align with these studies. We detected HlpA both in the extracellular medium and in cell envelopes fractions of *S. suis* (Fig. 1D). However, proteinase K accessibility assays evidenced that HlpA is not surface-exposed (Fig. 1E), possibly because of the absence of a specific membrane binding receptor as in other species. Its presence in the cell envelopes may instead relate to an unidentified secretion mechanism. In this work we generated an anti-HlpA antibody. This antibody reacted well with purified recombinant HlpA protein and recognized HlpA-GFP fusion protein, but hardly detected the native protein in several preparations of the wild-type strain. One possible explanation is that the highly basic nature of HlpA (pI 9.7) or its small size (9.4 kDa) affects transfer efficiency, whereas fusion with sfGFP may alter the overall charge and improve its detectability in Western blot assays.

HlpA homologous may contribute to bacterial virulence. For instance, *Streptococcus gallolyticus* produces a HlpA protein that binds to heparin (Boleij et al., 2009), and thus could enhance bacterial resistance to serum. Similar to other histone-like proteins, such as H-NS in *Actinobacillus pleuropneumoniae* or in *Hemophilus influenzae* (Dalai et al., 2009; Devaraj et al., 2018), HlpA may also contribute to biofilm formation and pathogenesis. While such roles remain unconfirmed in *S. suis*, our fluorescent mutants adhered to eukaryotic cells, formed biofilms, colonized mouse nostrils, and disseminated in a murine infection model. These results suggest that fusion of sfGFP to HlpA does not impair putative virulence-associated functions of the native protein.

In conclusion, our work demonstrates that fusing HlpA-sfGFP provides a robust method for generating bright, genetically stable *S. suis* strains suitable for detailed investigations of bacterial behavior in both in vitro and in vivo environments. Furthermore, these strains have proven to be valuable tools for evaluating novel virulence factors (Bosch et al., 2025). We anticipate that this system will enhance future research into *S. suis* pathogenesis and host-pathogen interactions.

CRediT authorship contribution statement

Carla García: Writing – review & editing, Methodology, Investigation. **Luis Saralegui:** Writing – original draft, Methodology, Investigation, Formal analysis, Data curation. **Camila Bosch:** Methodology, Investigation. **Paula Jurado:** Writing – review & editing, Methodology, Investigation. **Vloet Wessel:** Methodology, Investigation. **Marga van Setten:** Methodology, Investigation. **Rocío Bermúdez:** Resources, Methodology, Investigation. **Jesús Arenas:** Writing – review & editing, Supervision, Project administration, Funding acquisition, Conceptualization. **Clara Marín:** Writing – review & editing, Supervision, Resources, Methodology.

Funding

This work was supported by the Ciencia e Innovación/Agencia Española de Investigación MCIN/AEI/10.13039/501100011033 and, as appropriate, by ERDF A way of making Europe by the European Union or by the European Union NextGenerationEU/PRTR (Grant agreement PID2023–146823OB-I00), and fSs (Grant agreement 1600001704) funded by WBVR to Jesús Arenas. The funders had no role in study design, data collection and analysis, decision to publish, or preparation of the manuscript.

Declaration of Competing Interest

The authors declare no conflict of interest.

Acknowledgements

We would like to thank Lars Ravesloot (WBVR) for his assistance with the flow cytometry analysis. We also thank WBVR for providing the *S. suis* strain 10 and J28 and Dr. Virginia Aragón (CRESA) for providing strain P1/7. We would like to thank Mateo del Pozo (Labopat, Spain), Maria Casas Amorieta (Ovislab, Spain), and Ana Fernandez and Jose L Arnal (Exopol, Spain) for kindly provide *S. suis* invasive isolates Ss_2, Ss_45, Ss_64, Ss_72, Ss_105, Ss_106, Ss_121, Ss_134 used in this study for research.

Appendix A. Supporting information

Supplementary data associated with this article can be found in the online version at doi:10.1016/j.vetmic.2026.110964.

References

Neila-Ibáñez, C., Casal, J., Hennig-Pauka, I., Stockhofe-Zurwieden, N., Gottschalk, M., Migura-García, L., et al., 2021. Stochastic assessment of the economic impact of *Streptococcus suis*-associated disease in German, Dutch and Spanish swine farms. Front. Vet. Sci. 8, 676002. https://doi.org/10.3389/fvets.2021.676002.

Vötsch, D., Willenborg, M., Weldearegay, Y.B., Valentin-Weigand, P., 2018. *Streptococcus suis* - The "two faces" of a pathobiont in the porcine respiratory tract. Front. Microbiol. 9, 480. https://doi.org/10.3389/fmicb.2018.00480.

Huong, V.T.L., Ha, N., Huy, N.T., Horby, P., Nghia, H.D.T., Thiem, V.D., et al., 2014. Epidemiology, clinical manifestations, and outcomes of *Streptococcus suis* infection in humans. Emerg. Infect. Dis. 20 (7), 1105–1114. https://doi.org/10.3201/eid2007.131594.

Brizuela, J., Roodsant, T.J., Hasnoe, Q., van der Putten, B.C.L., Kozakova, J., Slotved, H. C., et al., 2024. Molecular epidemiology of underreported emerging zoonotic pathogen *Streptococcus suis* in Europe. Emerg. Infect. Dis. 30 (3), 413–422. https://doi.org/10.3201/eid3003.230348.

Goyette-Desjardins, G., Auger, J.P., Xu, J., Segura, M., Gottschalk, M., 2014. *Streptococcus suis*, an important pig pathogen and emerging zoonotic agent—an update on the worldwide distribution based on serotyping and sequence typing. Emerg. Microbes Infect. 3 (1), 1–20. https://doi.org/10.1038/emi.2014.45.

Uruén, C., García, C., Fraile, L., Tommassen, J., Arenas, J., 2022. How *Streptococcus suis* escapes antibiotic treatments. Vet. Res. 53, 91. https://doi.org/10.1186/s13567-022-01111-3.

Segura, M., 2015. *Streptococcus suis* vaccines: Candidate antigens and progress. Expert Rev. Vaccin. 14 (12), 1587–1608. https://doi.org/10.1586/14760584.2015.1101349.

Corsaut, L., Misener, M., Canning, P., Beauchamp, G., Gottschalk, M., Segura, M., 2020. Field study on the immunological response and protective effect of a licensed autogenous vaccine to control *Streptococcus suis* infections in post-weaned piglets. Vaccines 8, 384. https://doi.org/10.3390/vaccines8030384.

Rieckmann, K., Pendzialek, S.M., Vahlenkamp, T., Baums, C.G., 2020. A critical review speculating on the protective efficacies of autogenous *Streptococcus suis* bacterins as used in Europe. Porc. Health Manag. 6, 12. https://doi.org/10.1186/s40813-020-00150-6.

Weinert, L.A., Chaudhuri, R.R., Wang, J., Peters, S.E., Corander, J., Jombart, T., et al., 2015. Genomic signatures of human and animal disease in the zoonotic pathogen *Streptococcus suis*. Nat. Commun. 6, 6740. https://doi.org/10.1038/ncomms7740.

Guo, G., Du, D., Yu, Y., Zhang, Y., Qian, Y., Zhang, W., 2021. Pan-genome analysis of *Streptococcus suis* serotype 2 revealed genomic diversity among strains of different virulence. Transbound. Emerg. Dis. 68, 637–647. https://doi.org/10.1111/tbed.13725.

Uruén, C., Fernandez, A., Arnal, J.L., Del Pozo, M., Amoribieta, M.C., de Blas, I., et al., 2024. Genomic and phenotypic analysis of invasive *Streptococcus suis* isolated in Spain reveals genetic diversification and associated virulence traits. Vet. Res. 55, 11. https://doi.org/10.1186/s13567-024-01267-0.

Fittipaldi, N., Segura, M., Grenier, D., Gottschalk, M., 2012. Virulence factors involved in the pathogenesis of the infection caused by the swine pathogen and zoonotic agent *Streptococcus suis*. Future Microbiol 7 (2), 259–279. https://doi.org/10.2217/fmb.11.1.

Uruén, C., Chopo-Escuin, G., Tommassen, J., Mainar-Jaime, R.C., Arenas, J., 2020. Biofilms as promoters of bacterial antibiotic resistance and tolerance. Antibiotics 10 (1), 3. https://doi.org/10.3390/antibiotics.

Kjos, M., Aprianto, R., Fernandes, V.E., Andrew, P.W., van Strijp, J.A.G., Nijland, R., et al., 2015. Bright fluorescent *Streptococcus pneumoniae* for live-cell imaging of host-pathogen interactions. J. Bacteriol. 197 (5), 807–818. https://doi.org/10.1128/JB.02221-14.

Pédelacq, J.D., Cabantous, S., Tran, T., Terwilliger, T.C., Waldo, G.S., 2006. Engineering and characterization of a superfolder green fluorescent protein. Nat. Biotechnol. 24, 79–88. https://doi.org/10.1038/nbt1172.

Pettijohn, D.E., 1988. Histone-like proteins and bacterial chromosome structure. J. Biol. Chem. 263 (26), 12793–12796. https://doi.org/10.1016/S0021-9258(18)37625-7.

Dorman, C.J., Deighan, P., 2003. Regulation of gene expression by histone-like proteins in bacteria. Curr. Opin. Genet. Dev. 13 (2), 179–184. https://doi.org/10.1016/S0959-437X(03)00025-X.

Clifton-Hadley, F.A., 1984. Studies of *Streptococcus suis* type 2 infection in pigs. Vet. Res. Commun. 8, 217–227. https://doi.org/10.1007/BF02214715.

Wisselink, H.J., Reek, F.H., Vecht, U., Stockhofe-Zurwieden, N., Smits, M.A., E. Smith, H., 1999. Detection of virulent strains of *Streptococcus suis* type 2 and highly virulent strains of *Streptococcus suis* type 1 in tonsillar specimens of pigs by PCR. Vet. Microbiol. 67 (2), 143–157. https://doi.org/10.1016/S0378-1135(99)00036-X.

García López, C., Saralegui Remón, L., Uruén García, C., Jurado Romero, P., Gottschalk, M., Bosch Díaz, C., et al., 2024. Techniques for genetic manipulation. Methods Mol. Biol. 2815, 37–49. https://doi.org/10.1007/978-1-0716-3898-9_4.

Arenas, J., de Maat, V., Catón, L., Krekorian, M., Herrero, J.C., Ferrara, F., et al., 2015a. Fratricide activity of MafB protein of *N. meningitidis* strain B16B6. BMC Microbiol 5 15, 156. https://doi.org/10.1186/s12866-015-0493-6.

Arenas, J., Cano, S., Nijland, R., van Dongen, V., Rutten, L., van der Ende, A., et al., 2015b. The meningococcal autotransporter AutA is implicated in autoaggregation and biofilm formation. Environ. Microbiol. 17 (4), 1321–1337. https://doi.org/10.1111/1462-2920.12581.

Arenas, J., Paganelli, F.L., Rodríguez-Castaño, P., Cano-Crespo, S., van der Ende, A., van Putten, J.P.M., et al., 2016. Expression of the gene for autotransporter AutB of *Neisseria meningitidis* affects biofilm formation and epithelial transmigration. Front. Cell. Infect. Microbiol. 6, 162. https://doi.org/10.3389/fcimb.2016.00162.

Arenas, J., Abel, A., Sánchez, S., Marzoa, J., Berrón, S., van der Ley, P., et al., 2008. A cross-reactive neisserial antigen encoded by the NMB0035 locus shows high sequence conservation but variable surface accessibility. J. Med Microbiol 57, 80–87. https://doi.org/10.1099/jmm.0.47172-0.

Jurado, P., Uruén, C., Martínez, S., Lain, E., Sánchez, S., Rezusta, A., et al., 2023. Essential oils of *Pinus sylvestris*, *Citrus limon* and *Origanum vulgare* exhibit high bactericidal and anti-biofilm activities against *Neisseria gonorrhoeae* and *Streptococcus suis*. Biomed. Pharmacother. 168, 115703. https://doi.org/10.1016/j.biopha.2023.115703.

Seitz, M., Beineke, A., Seele, J., Fulde, M., Valentin-Weigand, P., Baums, C.G., 2012. A novel intranasal mouse model for mucosal colonization by *Streptococcus suis* serotype 2. J. Med. Microbiol. 61 (9), 1311–1318. https://doi.org/10.1099/jmm.0.043885-0.

Heydorn, A., Nielsen, A.T., Hentzer, M., Sternberg, C., Givskov, M., Ersbøll, B.K., et al., 2000. Quantification of biofilm structures by the novel computer program COMSTAT. Microbiol. (Read.) 146 (10), 2395–2407. https://doi.org/10.1099/00221287-146-10-2395.

Wrobel, A., Saragliadis, A., Pérez-Ortega, J., Sittman, C., Göttig, S., Liskiewicz, K., et al., 2020. The inverse autotransporters of *Yersinia ruckeri*, YrInv and YrIlm, contribute to biofilm formation and virulence. Environ. Microbiol 22 (7), 2939–2955. https://doi.org/10.1111/1462-2920.15051.

Chen, T., Huang, Q., Li, Z., Zhang, W., Lu, C., Yao, H., 2012. Construction and characterization of a *Streptococcus suis* serotype 2 recombinant expressing enhanced green fluorescent protein. PLoS One 7 (7), e3969. https://doi.org/10.1371/journal.pone.0039697.

Gilmer, D.B., Schmitz, J.E., Thandar, M., Euler, C.W., Fischetti, V.A., 2017. The phage lysin PlySs2 Decolonizes *Streptococcus suis* from murine intranasal mucosa. PLoS One 12 (1), e0169180. https://doi.org/10.1371/journal.pone.0169180.

Smith, H.E., Damman, M., Van Der Velde, J., Wagenaar, F., Wisselink, H.J., Stockhofe-Zurwieden, N., Smits, M.A., 1999. Identification and characterization of the *cps* locus of *Streptococcus suis* serotype 2: the capsule protects against phagocytosis and is an important virulence factor. Infect. Immun. 67 (4), 1750–1756. https://doi.org/10.1128/iai.67.4.1750-1756.1999.

García, C., Saralegui, L., Morales, B., Jurado, P., Bes, M.T., Marín, C., et al., 2026. Identification of ShgH as a dual histidine/glutamine transporter component essential for *Streptococcus suis* virulence and biofilm modulation. Microbiol. Res. 302, 128354. https://doi.org/10.1016/j.micres.2025.128354.

Aymanns, S., Mauerer, S., van Zandbergen, G., Wolz, C., Spellerberg, B., 2011. High-level fluorescence labeling of Gram-positive pathogens. PLoS One 6 (6), e19822. https://doi.org/10.1371/journal.pone.0019822.

Aspiras, M.B., Kazmerzak, K.M., Kolenbrander, P.E., Mcnab, R., Hardegen, N., Jenkinson, H.F., 2000. Expression of green fluorescent protein in *Streptococcus gordonii* DL1 and its use as a species-specific marker in coadhesion with *Streptococcus oralis* 34 in saliva-conditioned biofilms in vitro. Appl. Environ. Microbiol. 66 (9), 4074–4083. https://doi.org/10.1128/AEM.66.9.4074-4083.2000.

Mu, R., Anderson, D., Merritt, J., Wu, H., Kreth, J., 2021. Post-translational modification of *Streptococcus sanguinis* SpxB influences protein solubility and H_2O_2 production. Mol. Oral. Microbiol. 36 (5), 267–277. https://doi.org/10.1111/omi.12348.

Lautenschläger, N., Schmidt, K., Schiffer, C., Wulff, T.F., Hahnke, K., Finstermeier, K., et al., 2024. Expanding the genetic toolbox for the obligate human pathogen *Streptococcus pyogenes*. Front. Bioeng. Biotechnol. 12, 1395659. https://doi.org/10.3389/fbioe.2024.1395659.

Odo, C.M., Vega, L.A., Mukherjee, P., DebRoy, S., Flores, A.R., Shelburne, S.A., 2024. Emergent emm4 group A *Streptococcus* evidences a survival strategy during interaction with immune effector cells. Infect. Immun. 92 (7), e0015224. https://doi.org/10.1101/2024.04.09.588776.

Lun, S., Willson, P.J., 2004. Expression of green fluorescent protein and its application in pathogenesis studies of serotype 2 *Streptococcus suis*. J. Microbiol. Methods 56 (3), 401–412. https://doi.org/10.1016/j.mimet.2003.11.012.

Xu, L., Lin, L., Lu, X., Xiao, P., Liu, R., Wu, M., et al., 2021. Acquiring high expression of suilysin enables non-epidemic *Streptococcus suis* to cause streptococcal toxic shock-like syndrome (STSLS) through NLRP3 inflammasome hyperactivation. Emerg. Microbes Infect. 10 (1), 1309–1319. https://doi.org/10.1080/22221751.2021.1908098.

Zhang, D., Du, N., Ma, S., Hu, Q., Lu, G., Chen, W., et al., 2014. In vitro transcriptome analysis of two Chinese isolates of *Streptococcus suis* serotype 2. Genom. Proteom. Bioinform. 12 (6), 266–275. https://doi.org/10.1016/j.gpb.2014.11.001.

Arenas, J., Bossers-de Vries, R., Harders-Westerveen, J., Buys, H., Ruuls-van Stalle, L.M. F., Stockhofe-Zurwieden, N., et al., 2019. In vivo transcriptomes of *Streptococcus suis* reveal genes required for niche-specific adaptation and pathogenesis. Virulence 10 (1), 334–351. https://doi.org/10.1080/21505594.2019.1599669.

Severin, A., Nickbarg, E., Wooters, J., Quazi, S.A., Matsuka, Y.V., Murphy, E., et al., 2007. Proteomic analysis and identification of *Streptococcus pyogenes* surface-associated proteins. J. Bacteriol. 189 (5), 1514–1522. https://doi.org/10.1128/JB.01132-06.

Katsube, T., Matsumoto, S., Takatsuka, M., Okuyama, M., Ozeki, Y., Naito, M., et al., 2007. Control of cell wall assembly by a histone-like protein in mycobacteria. J. Bacteriol. 189 (22), 8241–8249. https://doi.org/10.1128/jb.00550-07.

Stinson, M.W., Mclaughlin, R., Suk, H.O., Juarez, Z., Barnard, E., 1998. Streptococcal histone-like protein: primary structure of hlpA and protein binding to lipoteichoic acid and epithelial cells. Infect. Immun. 66 (1), 259–265. https://doi.org/10.1128/iai.66.1.259-265.1998.

Kim, N., Weeks, D.L., Shin, J.M., Scott, D.R., Young, M.K., Sachs, G., 2002. Proteins released by *Helicobacter pylori* in vitro. J. Bacteriol. 184 (22), 6155–6162. https://doi.org/10.1128/JB.184.22.6155-6162.2002.

Boleij, A., Schaeps, R.M.J., De Kleijn, S., Hermans, P.W., Glaser, P., Pancholi, V., et al., 2009. Surface-exposed histone-like protein A modulates adherence of *Streptococcus gallolyticus* to colon adenocarcinoma cells. Infect. Immun. 77 (12), 5519–5527. https://doi.org/10.1128/IAI.00384-09.

Dalai, B., Zhou, R., Wan, Y., Kang, M., Li, L., Li, T., et al., 2009. Histone-like protein H-NS regulates biofilm formation and virulence of *Actinobacillus pleuropneumoniae*. Microb. Pathog. 46 (3), 128–134. https://doi.org/10.1016/j.micpath.2008.11.005.

Devaraj, A., Buzzo, J., Rocco, C.J., Bakaletz, L.O., Goodman, S.D., 2018. The DNABII family of proteins is comprised of the only nucleoid associated proteins required for nontypeable *Haemophilus influenzae* biofilm structure. MicrobiologyOpen 7 (3), e00563. https://doi.org/10.1002/mbo3.563.

Bosch, C., García, C., Saralegui, L., van Beek, L., de Jonge, M.I., Marín, C., Arenas, J., 2025. Identification of the methionine transporter MetQ in *Streptococcus suis* and its contribution to virulence and biofilm formation. Vet. Res. 56 (1), 99. https://doi.org/10.1186/s13567-025-01522-y.

Wisselink, H.J., Smith, H.E., Stockhofe-Zurwieden, N., Peperkamp, K., 2000. U. Vecht, Distribution of capsular types and production of muramidase-released protein (MRP) and extracellular factor (EF) of *Streptococcus suis* strains isolated from diseased pigs in seven European countries. Vet. Microbiol. 74 (3), 237–248. https://doi.org/10.1016/S0378-1135(00)00188-7.

Weingartl, H.M., Sabara, M., Pasick, J., Van Moorlehem, E., Babiuk, L., 2002. Continuous porcine cell lines developed from alveolar macrophages: partial characterization and virus susceptibility. J. Virol. Methods 104 (2), 203–216. https://doi.org/10.1016/S0166-0934(02)00085-X.